Photochemistry and Photobiology, 2019, 95: 1441–1445

Optical Spectroscopy as a Method for Skin Cancer Risk Assessment

Eladio Rodriguez-Diaz[1], Danielle Manolakos[2], Holly Christman*[3,4], Michael A. Bonning[4,5], John K. Geisse[3,6], Ousama M. A'Amar[1], David J. Leffell[7] and Irving J. Bigio[1,8]

[1]Department of Biomedical Engineering, Boston University, Boston, MA
[2]Gold Coast Dermatology Center, Delray Beach, FL
[3]Department of Dermatology, University of California, San Francisco, San Francisco, CA
[4]DermaSensor, Inc., Miami, FL
[5]Department of Health Systems and Populations, Macquarie University, Sydney, NSW, Australia
[6]Department of Pathology, University of California, San Francisco, San Francisco, CA
[7]Yale University School of Medicine, New Haven, CT
[8]Departments of Electrical & Computer Engineering, Physics, Medicine, Boston University, Boston, MA

Received 6 March 2019, accepted 24 June 2019, DOI: 10.1111/php.13140

ABSTRACT

Skin cancer is the most prevalent cancer, and its assessment remains a challenge for physicians. This study reports the application of an optical sensing method, elastic scattering spectroscopy (ESS), coupled with a classifier that was developed with machine learning, to assist in the discrimination of skin lesions that are concerning for malignancy. The method requires no special skin preparation, is non-invasive, easy to administer with minimal training, and allows rapid lesion classification. This novel approach was tested for all common forms of skin cancer. ESS spectra from a total of 1307 lesions were analyzed in a multi-center, non-randomized clinical trial. The classification algorithm was developed on a 950-lesion training dataset, and its diagnostic performance was evaluated against a 357-lesion testing dataset that was independent of the training dataset. The observed sensitivity was 100% (14/14) for melanoma and 94% (105/112) for non-melanoma skin cancer. The overall observed specificity was 36% (84/231). ESS has potential, as an adjunctive assessment tool, to assist physicians to differentiate between common benign and malignant skin lesions.

INTRODUCTION

Skin cancer is the most prevalent cancer, and its clinical diagnosis remains a challenge for physicians (1,2). The incidence of both melanoma and non-melanoma skin cancer (NMSC) is increasing, especially in individuals with fair skin (3–6). In the United States, there are an estimated 5.4 million new cases of skin cancer every year (7). Early diagnosis of suspicious lesions is critical in reducing morbidity and mortality related to skin cancers, especially to melanoma (7–9). However, the identification of skin cancers requires expertise and experience. Clinical signs of early melanoma can be ambiguous, even to the most experienced dermatologist. As a result of this clinical need, various devices have been developed to aid the clinician in deciding whether a lesion requires biopsy or follow-up care (10–14). While many of those diagnostic aids have shown promising results, there are still challenges to their widespread implementation (14). These devices have focused on either melanoma or NMSC, rather than all common cancer types. The narrow clinical scope, high cost of some technologies, slow speed and/or complicated output have limited their usefulness to dermatologists, and no such device has been developed and approved by the FDA for use in the primary care setting. As value-based interventions drive healthcare delivery strategies, the goal of effective lesion triage will likely increase in importance (15–17). To encourage widespread use, especially at the primary care level, new tools are needed that provide accurate information in a simple, cost-effective, and time-efficient manner.

Elastic Scattering Spectroscopy (ESS) is a specific form of sub-diffuse reflectance spectroscopy (18), in which the spectral recording of photons scattered back from refractive-index gradients is associated with the micro- and nano-scale structures in tissue (19). The backscattered intensity is plotted against wavelength for a broad spectral range (330–850 nm for the work reported here); the spectrum is altered by the disease-associated changes that occur within tissue, both at a cellular and a subcellular level (19). ESS requires no skin preparation and is easy to administer, requiring minimal practitioner training. Due to its ability to translate tissue morphology into spectral features at the cellular and sub-cellular levels, ESS relates directly to the observed tissue architecture and structure of histopathologic features (20,21). Different tissue types and histopathological status exhibit specific optical signatures, and ESS has been demonstrated clinically to assess malignancy in multiple tissue types (20–27). Spectral correlation with histopathologic diagnosis using variations of ESS has also been reported by other groups (28,29).

Here, we describe the development of an unsupervised, statistical classification approach for the development of a machine learning algorithm to be used on ESS measurements to assess melanoma and NMSC skin cancers. The results demonstrate that a spectroscopic algorithm can evaluate all common types of skin cancer simultaneously.

*Corresponding author email: holly.christman@dermasensor.com (Holly Christman)

MATERIALS AND METHODS

Ethical conduct. The guidelines of the revised Declaration of Helsinki, the Guidelines of Good Clinical Practice (ISO-14155), and the requirements of national and data protection laws were followed. The study was approved by the Western Institutional Review Board (Protocol #20150755).

Objectives. The aim of this clinical study was to develop a spectral classification algorithm using ESS measurements to distinguish between the most common types of malignant and benign skin lesions.

The dichotomous categories of "high risk" and "low risk" were used to group the output of the ESS classifier, combining all sub-types of skin cancer and benign lesions as two classifications. The sensitivity and specificity of the ESS measurements and classifier were validated against histopathologic diagnosis.

Safety. The Western Investigational Review Board designated the ESS system as non-significant risk due to the non-invasive nature of the optical measurements and the low levels of radiant exposure. The safety of the ESS device was evaluated by recording all adverse events reported for study participants. No adverse events were reported for study participants in the course of the study.

Study design and data acquisition. Recruitment into this investigator-blinded multi-center study was conducted at four private-practice investigational dermatology sites between 2015 and 2018. Potential study participants were screened according to the study's inclusion and exclusion criteria described in Table 1. Subsequent to written informed consent, a medical history was completed and a clinical evaluation including full body skin check was performed. Each lesion was photographed prior to ESS measurements, and the photos were stored for future research. Eligible lesions were biopsied, following standard practice, and assessed histopathologically. Up to five ESS measurements were made in all lesions, regardless of size. Each measurement was classified separately, and their aggregate score was used to classify the lesion. The variability of spectra within individual lesions was not assessed in this study. ESS measurements were then correlated with histopathologic diagnosis. In a procedure implemented later in the study, dermatologist-identified unbiopsied benign lesions from consented patients were also measured with ESS, for classifier training on a dataset that is representative of the lesions commonly encountered in clinical practice. Expert-diagnosed benign lesions were also included in the testing set on which the algorithm's performance was determined.

Inclusion and exclusion criteria. Patients with skin lesions suggestive of risk for skin cancer were invited to participate in the study. To minimize selection bias, all lesions for which biopsy or excision was clinically indicated were eligible for inclusion in the study. From consented patients, other lesions that were deemed by the dermatologist to be benign without biopsy confirmation were measured with the ESS system and included in the machine-learning training or testing dataset. The inclusion and exclusion criteria are listed in Table 1.

Blinding. The study was blinded for both patients and investigators, as no classifier output was displayed on the device.

Table 1. Study inclusion and exclusion criteria.

Inclusion criteria:

- Subjects undergoing a skin biopsy or excision of a suspicious lesion (skin cancer).
- Subjects with lesions clinically deemed benign, and not biopsied or excised.
- Both sexes and adults above age 16 years.
- Able to give informed consent

Exclusion criteria:

- Recent intense UV exposure, *e.g.* sunburn, tanning, in the week prior.
- Pregnancy.
- Unable to give informed consent.

Elastic scattering spectroscopy measurements. The ESS device uses a broadband xenon light-source (Perkin Elmer, Inc. or Hamamatsu, Inc.) that emits short pulses of light (~30 microseconds in duration) that span wavelengths from near-ultraviolet, through visible, to near-infrared (300–900 nm). The spectrometer invokes a detector array (Hamamatsu, Inc.) incorporating a fast electronic shutter. The short pulse, coupled with time-gated detection, enables system performance that is not affected by room light, thus not requiring a dark environment for recording the optical spectra.

The fiber-optic probe comprises two adjacent optical fibers, enclosed in a small tip that is placed in contact with the lesion surface. The fiber probe tip, which only transfers and collects light and does not invoke any electrical elements, is the only component that makes contact with the subject's skin. The skin-specific optical geometry for ESS measurements was determined by preliminary studies in an animal model (30) and with Monte Carlo simulations of light propagation in skin. A 400-micron diameter illumination fiber is coupled to the pulsed light source to illuminate a small volume of the tissue. An adjacent 200-micron diameter fiber collects backscattered light from the tissue and is coupled to the optical spectrometer to record the wavelengths that are backscattered. The illumination and collection fibers are bonded in the tip of the probe and have a ~360-micron center-to-center separation.

Data processing and analysis. All ESS spectra were pre-processed prior to analysis. Raw measurements consist of 1347 bands, corresponding to the pixel density of the detector in the spectrometer, between the wavelength range of 300–900 nm. Before analysis, each spectrum was smoothed and down-sampled by averaging blocks of ~2 bands, resulting in a spectrum of 601 bands in the wavelength range of 300–900 nm. Dimensionality was further reduced by limiting the spectral range to be analyzed to 360–820 nm and by using smoothing Gaussian filters with 15-nm full-width-half-max every 10 nm in the 360–820-nm range, resulting in a spectrum of 47 bands. These pre-processing steps were performed to reduce high-frequency noise variations and to remove the regions of the spectra with low signal-to-noise ratios arising from combined detector sensitivity and lower source light intensity at the extremes of its output spectrum. Finally, individual spectra were then normalized to the area under the trace, to enable analysis based on spectral shape, independent of relative intensities (see Fig. 1).

Convolutional neural networks (CNN, or ConvNet) were used to build dichotomous classification algorithms that differentiate measured ESS spectra as corresponding either to a malignant or benign lesion. The malignant/benign designations were obtained from histology of the biopsied lesions and were correlated with spectral measurements for algorithm design and validation. The dichotomous classifier category of "high risk" lesions included histologically-proven melanoma and NMSC; the "low risk" category included all other lesions. The method does not differentiate between melanocytic/non-melanocytic or pigmented/non-pigmented lesions. All malignant lesions and all benign lesions were combined for the sensitivity and specificity analyses. The ConvNet consisted of four convolutional layers, with 5×1 filters in the first three layers and a 3×1 filter in the last layer, leaky rectified linear unit (ReLU) activation with gradients of 0.5, maxpooling sub-sampling, with stochastic gradient-descent with momentum (SGDM) optimization. The output consisted of a fully-connected layer, with dropout applied to minimize over-fitting. A training dataset consisting of over 4200 ESS measurements from 950 skin lesions was used to tune classifier parameters, including the receiver-operating-characteristic (ROC) curve operating point. Sensitivity and specificity were the primary performance measures. Exact binomial confidence-intervals of 95% are provided with reported performance estimates.

RESULTS

Lesions for testing and training

The training dataset contained 950 lesions contributing more than 4200 spectra. The 787 patients enrolled in the study were predominantly male (64.7%) with a mean age of 61.3 years. Patients had Fitzpatrick Skin Type 1 or 2 in 63.9% of cases, and 35.1% had Fitzpatrick Type 3 skin. For the algorithm testing dataset, presented here, 357 lesions from this study (not included

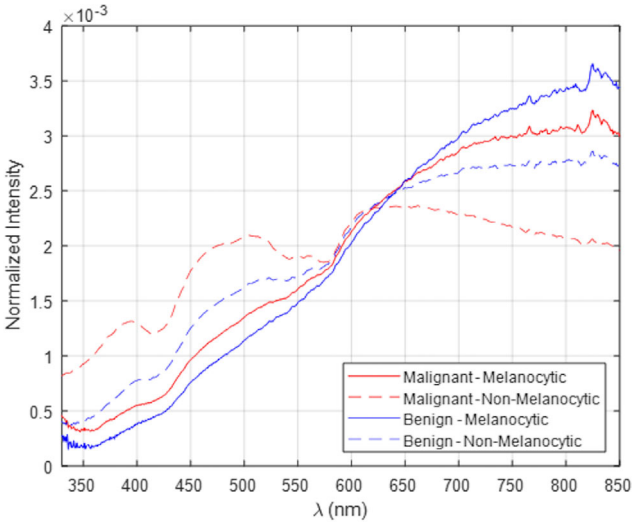

Figure 1. Differentiated average spectral signatures for all training dataset lesions grouped by histopathologic assignment.

in the training set) were used. That is, the training and testing datasets were independent, and were chosen randomly. A total of 23 patients contributed more than one malignant lesion to the testing set –one with six malignant lesions and 22 with up to four malignant lesions. The maximum number of biopsied lesions contributed by a single participant was six. All lesions were considered independent for this study.

Performance results

The dichotomous outputs of the ESS algorithm were compared with the histopathologic diagnoses. Of the 357 lesions (Table 2), 126 were histologically classified as malignant. Of these malignant lesions, 14 (11%) were melanoma and 112 (89%) were NMSC. The classifier for ESS correctly identified 14 of the 14 melanomas and 105 of the 112 NMSCs as "high risk". The combined sensitivity of the classifier was 94%. Four severely dysplastic melanocytic lesions were reported separately in the final performance tables and excluded from the analysis, due to the low number of lesions and the fact that there was significant inconsistency of diagnosis among the histopathologists. The classifier reported two of the four of this sub-set as "high risk". Of the 231 benign lesions, the classifier correctly identified 84 as "low risk", yielding an overall specificity of 36%. Classifier specificity for histology-proven mildly atypical melanocytic lesions was 69% (18/26).

DISCUSSION

Melanoma and non-melanoma skin cancer represent an increasing public health challenge (7). Early detection of melanoma remains the most effective strategy to reduce morbidity and mortality (31). Nonetheless, the equivocal nature of many lesions can make early clinical diagnosis difficult (30,32,33).

The ESS device and a trained classification algorithm were used to distinguish between benign and malignant skin lesions based on the spectral features of elastically-scattered light, demonstrating the potential to differentiate benign and malignant lesions and to provide accurate, reproducible information to aid physicians in assessing skin lesions for malignancy. We have shown that the ESS measurements can be used as inputs for a classification algorithm for the most common skin cancers. The technology requires no skin preparation and generates a simple dichotomous output in a non-invasive way. Importantly, this is accomplished for all skin lesions, and is not limited to a pigmented subset. The statistical learning approach used here has also been shown to perform well when assessing other skin lesion datasets, based on photographic images (34,35).

Challenges remain to further develop the classifier algorithm. Classifiers in general are limited by a less-than-perfect gold standard: a degree of discordance among dermatopathologists in the evaluation of biopsy specimens of pigmented lesions. This well-documented inconsistency can be significant when distinguishing microscopic features of dysplastic nevi, melanoma *in situ* and early-stage invasive melanoma (36–38). In this study, approximately one-third of lesions designated as severely dysplastic were either downgraded or upgraded when overread by another dermatopathologist, something not uncommon for this type of lesion.

The lack of universal agreement about the histopathologic interpretation of certain categories of skin lesions is a special concern, since published studies often rely on "known" histologic diagnoses of biopsied lesions. This results in classifiers that are undertrained on lesions unlikely to be biopsied, such as those that appear to be clinically benign. Nonetheless, the inclusion of dermatologist-identified unbiopsied lesions in the classifier

Table 2. Classifier performance on the testing dataset.

Histological assignment		Se	TP	FN	Total	LCB	UCB
	Overall Sensitivity	**0.94**	**119**	**7**	**126**	**0.89**	**0.98**
Melanocytic – Malignant	Melanoma	1.00	14	0	14	0.77	1.00
Non-Melanocytic – Malignant	All NMSC	0.94	105	7	112	0.88	0.97
	BCC	0.94	64	4	68	0.86	0.98
	SCC	0.93	40	3	43	0.81	0.99
Melanocytic – Highly atypical		0.50	2	2	4	0.07	0.93

		Sp	TN	FP	Total	LCB	UCB
Benign	**Overall Specificity**	**0.36**	**84**	**147**	**231**	**0.30**	**0.43**
	Actinic keratosis	0.07	2	26	28	0.01	0.24
	Seborrheic keratosis	0.30	11	26	37	0.16	0.47
	Mildly atypical nevi	0.69	18	8	26	0.48	0.86
	Clinically diagnosed benign lesions	0.42	46	63	109	0.33	0.52

TP = true positive; TN = true negative; FP = false positive; FN = false negative; LCB = lower confidence bound; UCB = upper confidence bound; NMSC = non-melanoma skin cancer (includes one lesion that is not BCC or SCC); BCC = basal cell carcinoma; SCC = squamous cell carcinoma. CI: 95%.

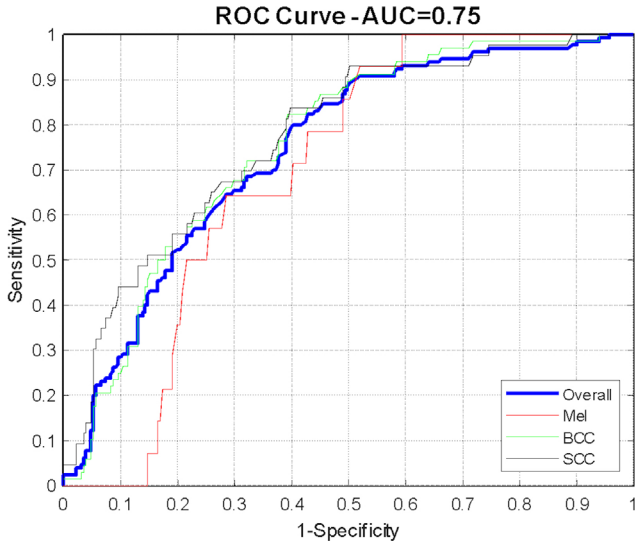

Figure 2. Receiver operating characteristic (ROC) curve for the binary classifier.

development creates a training dataset that is potentially more representative of lesions encountered in clinical practice, and for which such a technology would be clinically beneficial.

Another important aspect of this study is that all lesions were selected for biopsy by dermatologists. This selects for a population of lesions that are more likely to show some degree of cellular atypia even if they end up being classified histopathologically as benign. In the analysis of the ROC curve for the classification algorithm (Fig. 2) we can see a trade-off between sensitivity and specificity. Given the importance of identifying skin cancers, especially melanoma, the sensitivity of the device was purposefully set to a high value with a final sensitivity of 94% and specificity of 36%. In comparison, performance of physicians can vary greatly according to expertise (39). In primary care, performance was reported as 54.1% sensitivity and 71.3% specificity (39). Therefore, ESS may prove useful in primary care for aiding in the assessment of lesions suggestive of skin cancer and to improve referral of malignant skin lesions. Further studies are necessary in this context.

In conclusion, ESS measurements are effective in translating tissue morphology at the cellular and sub-cellular levels into spectral features, and permit the development of a meaningful classification algorithm for lesions with divergent pathological features. The previously well-established technical basis of ESS supports the findings of this study (20–29).

Further work is needed to refine the machine-learning classifier, to assess the lesion spectrum encountered in clinical practice, and to compare the performance of the device with the current standard of care. To validate these propositions, larger prospective studies are necessary.

Acknowledgements—We would like to thank Steven Hacker, Srdjan Prodanovich and Andrew Weinstein and their patients for their contributions to this study. This study was funded by DermaSensor Inc.

CONFLICTS OF INTEREST

Eladio Rodriguez-Diaz is a co-inventor, with fractional royalty rights, to the Boston University patents licensed to DermaSensor. Irving J Bigio is a member of the Scientific Advisory Board of DermaSensor Inc., with stock options, and is a co-inventor, with fractional royalty rights, to the Boston University patents licensed to DermaSensor. Holly Christman, John K Geisse and David J Leffell are members of the Scientific Advisory Board of DermaSensor and are compensated by the company. Michael A Bonning is a paid consultant of DermaSensor Inc., with stock options.

Danielle Manolakos and Ousama M A'Amar declare no conflicts of interest.

REFERENCES

1. Wilson, R. L., B. A. Yentzer, S. P. Isom, S. R. Feldman and A. B. Jr Fleischer (2012) How good are US dermatologists at discriminating skin cancers? A number-needed-to-treat analysis *J. Dermatolog. Treat.* **23**, 65–69.
2. Argenziano, G., L. Cerroni, I. Zalaudek, S. Staibano, R. Hofmann-Wellenhof, N. Arpaia, R. M. Bakos, B. Balme, J. Bandic, R. Bandelloni and A. M. Brunasso (2012) Accuracy in melanoma detection: A 10-year multicenter survey. *J. Am. Acad. Dermatol.* **67**, 54–59.
3. Robertson, F. M. and L. Fitzgerald (2017) Skin cancer in the youth population of the United Kingdom. *J. Cancer Policy* **12**, 67–71.
4. Lomas, A., J. Leonardi-Bee and F. Bath-Hextall (2012) A systematic review of worldwide incidence of nonmelanoma skin cancer. *Br. J. Dermatol.* **166**, 1069–1080.
5. Ackermann, E., D. Askew, I. D. Williams, P. Byrnes and G. K. Mitchell (2007) Management of skin cancer in Australia: A comparison of general practice and skin cancer clinics. *Aust. Fam. Physician* **36**, 1073–1075.
6. Belot, A., P. Grosclaude, N. Bossard, E. Jougla, E. Benhamou, P. Delafosse, A. V. Guizard, F. Molinié, A. Danzon, S. Bara and A. M. Bouvier (2008) Cancer incidence and mortality in France over the period 1980–2005. *Rev. Epidemiol. Sante Publique* **56**, 159–175.
7. Rogers, H. W., M. A. Weinstock, S. R. Feldman and B. M. Coldiron (2015) Incidence estimate of nonmelanoma skin cancer (keratinocyte carcinomas) in the US population. *J. Am. Acad. Dermatol.* **151**, 1081–1086.
8. Wernli, K. J., N. B. Henrikson, C. C. Morrison, M. Nguyen, G. Pocobelli and E. P. Whitlock (2016) Screening for Skin Cancer in Adults: An Updated Systematic Evidence Review for the US Preventive Services Task Force: Evidence Synthesis No. 137.
9. Glazer, A. M., R. R. Winkelmann, A. S. Farberg and D. S. Rigel (2012) Analysis of trends in US melanoma incidence and mortality. *J. Am. Acad. Dermatol.* **153**, 225–226.
10. Malvehy, J., A. Hauschild, C. Curiel-Lewandrowski, P. Mohr, R. Hofmann-Wellenhof, R. Motley, C. Berking, D. Grossman, J. Paoli, C. Loquai and J. Olah (2014) Clinical performance of the Nevisense system in cutaneous melanoma detection: An international, multicentre, prospective and blinded clinical trial on efficacy and safety. *Br. J. Dermatol.* **171**, 1099–1107.
11. Monheit, G., A. B. Cognetta, L. Ferris, H. Rabinovitz, K. Gross, M. Martini, J. M. Grichnik, M. Mihm, V. G. Prieto, P. Googe and R. King (2011) The performance of MelaFind: A prospective multicenter study. *Arch. Dermatol.* **147**, 188–194.
12. Emery, J. D., J. Hunter, P. N. Hall, A. J. Watson, M. Moncrieff and F. M. Walter (2010) Accuracy of SIAscopy for pigmented skin lesions encountered in primary care: Development and validation of a new diagnostic algorithm. *BMC Dermatol.* **10**, 9.
13. Ulrich, M., T. Von Braunmuehl, H. Kurzen, T. Dirschka, C. Kellner, E. Sattler, C. Berking, J. Welzel and U. Reinhold (2015) The sensitivity and specificity of optical coherence tomography for the assisted diagnosis of nonpigmented basal cell carcinoma: An observational study. *Br. J. Dermatol.* **173**, 428–435.
14. Higgins, H. W., K. C. Lee and D. J. Leffell (2014) Point of care cutaneous imaging technology in melanoma screening and mole mapping. *F1000Prime Rep.* **6**, 34.
15. Doran, C. M., R. Ling, J. Byrnes, M. Crane, A. Searles, D. Perez and A. Shakeshaft (2015) Estimating the economic costs of skin cancer in New South Wales, Australia. *BMC Public Health* **15**, 952.

16. Gordon, L. G. and D. Rowell (2015) Health system costs of skin cancer and cost-effectiveness of skin cancer prevention and screening: A systematic review. *Eur. J. Cancer Prev.* **24**, 141–149.
17. Elliott, T. M., D. C. Whiteman, C. M. Olsen and L. G. Gordon (2017) Estimated healthcare costs of melanoma in Australia over 3 years post-diagnosis. *Appl. Health Econ. Health Policy* **15**, 805–816.
18. Zonios, G., L. T. Perelman, V. Backman, R. Manoharan, M. Fitzmaurice, J. Van Dam and M. S. Feld (1999) Diffuse reflectance spectroscopy of human adenomatous colon polyps *in vivo*. *Appl. Opt.* **38**, 6628–6637.
19. Bigio, I. J. and J. R. Mourant (1997) Ultraviolet and visible spectroscopies for tissue diagnostics: Fluorescence spectroscopy and elastic-scattering spectroscopy. *Phys. Med. Biol.* **42**, 803.
20. Bigio, I. J., S. G. Bown, G. M. Briggs, C. Kelley, S. Lakhani, D. C. Pickard, P. M. Ripley, I. Rose and C. Saunders (2000) Diagnosis of breast cancer using elastic-scattering spectroscopy: Preliminary clinical results. *J. Biomed. Opt.* **5**, 221–229.
21. Suh, H., O. A'Amar, E. Rodriguez-Diaz, S. Lee, I. Bigio and J. E. Rosen (2011) Elastic light-scattering spectroscopy for discrimination of benign from malignant disease in thyroid nodules. *Ann. Surg. Oncol.* **18**, 1300–1305.
22. Mourant, J. R., I. J. Bigio, J. Boyer, R. L. Conn, T. Johnson and T. Shimada (1995) Spectroscopic diagnosis of bladder cancer with elastic light scattering. *Lasers Surg. Med.* **17**, 350–357.
23. Lovat, L. B., K. Johnson, G. D. Mackenzie, B. R. Clark, M. R. Novelli, S. Davies, M. O'Donovan, C. Selvasekar, S. M. Thorpe, D. Pickard and R. Fitzgerald (2006) Elastic scattering spectroscopy accurately detects high grade dysplasia and cancer in Barrett's oesophagus. *Gut* **55**, 1078–1083.
24. Keshtgar, M. R., D. W. Chicken, M. R. Austwick, S. K. Somasundaram, C. A. Mosse, Y. Zhu, I. J. Bigio and S. G. Bown (2010) Optical scanning for rapid intraoperative diagnosis of sentinel node metastases in breast cancer. *Br. J. Surg.* **97**, 1232–1239.
25. A'Amar, O. M., L. Liou, E. Rodriguez-Diaz, A. De las Morenas and I. J. Bigio (2013) Comparison of elastic scattering spectroscopy with histology in *ex vivo* prostate glands: Potential application for optically guided biopsy and directed treatment. *Lasers Med. Sci.* **28**, 1323–1329.
26. Rodriguez-Diaz, E., C. Atkinson, L. I. Jepeal, A. Berg, C. S. Huang, S. R. Cerda, M. J. O'Brien, I. J. Bigio, F. A. Farraye and S. K. Singh (2014) Elastic scattering spectroscopy as an optical marker of inflammatory bowel disease activity and subtypes. *Inflamm. Bowel Dis.* **20**, 1029–1036.
27. Rodriguez-Diaz, E., Q. Huang, S. R. Cerda, M. J. O'Brien, I. J. Bigio and S. K. Singh (2015) Endoscopic histological assessment of colonic polyps by using elastic scattering spectroscopy. *Gastrointest. Endosc.* **81**, 539–547.
28. Mostaço-Guidolin, L. B., L. S. Murakami, A. Nomizo and L. Bachmann (2009) Fourier transform infrared spectroscopy of skin cancer cells and tissues. *Appl. Spectrosc. Rev.* **44**, 438–455.
29. Qiu, L., D. K. Pleskow, R. Chuttani, E. Vitkin, J. Leyden, N. Ozden, S. Itani, L. Guo, A. Sacks, J. D. Goldsmith and M. D. Modell (2010) Multispectral scanning during endoscopy guides biopsy of dysplasia in Barrett's esophagus. *Nat. Med.* **16**, 603.
30. A'Amar, O. M., R. D. Ley and I. J. Bigio (2004) Comparison between ultraviolet-visible and near-infrared elastic scattering spectroscopy of chemically induced melanomas in an animal model. *J. Biomed. Opt.* **9**, 1320–1327.
31. Carli, P., P. Nardini, E. Crocetti, V. De Giorgi and B. Giannotti (2004) Frequency and characteristics of melanomas missed at a pigmented lesion clinic: A registry-based study. *Melanoma Res.* **14**, 403–407.
32. Corbo, M. D. and J. Wismer (2012) Agreement between dermatologists and primary care practitioners in the diagnosis of malignant melanoma: Review of the literature. *J. Cutan Med. Surg.* **16**, 306–310.
33. Mar, V. J., R. A. Scolyer and G. V. Long (2017) Computer-assisted diagnosis for skin cancer: Have we been outsmarted? *Lancet* **389**, 1962–1964.
34. Esteva, A., B. Kuprel, R. A. Novoa, J. Ko, S. M. Swetter, H. M. Blau and S. Thrun (2017) Dermatologist-level classification of skin cancer with deep neural networks. *Nature* **542**, 115.
35. Han, S. S., W. Lim, M. S. Kim, I. Park, G. H. Park and S. E. Chang (2018) Interpretation of the outputs of deep learning model trained with skin cancer dataset. *J. Invest Dermatol.* **138**, 2275.
36. Braun, R. P., D. Gutkowicz-Krusin, H. Rabinovitz, A. Cognetta, R. Hofmann-Wellenhof, V. Ahlgrimm-Siess, D. Polsky, M. Oliviero, I. Kolm, P. Googe and R. King (2012) Agreement of dermatopathologists in the evaluation of clinically difficult melanocytic lesions: How golden is the 'gold standard'? *Dermatology* **224**, 51–58.
37. Carney, P. A., L. M. Reisch, M. W. Piepkorn, R. L. Barnhill, D. E. Elder, S. Knezevich, B. M. Geller, G. Longton and J. G. Elmore (2016) Achieving consensus for the histopathologic diagnosis of melanocytic lesions: Use of the modified Delphi method. *J. Cutan. Pathol.* **43**, 830–837.
38. Kim, C. C., E. G. Berry, M. A. Marchetti, S. M. Swetter, G. Lim, D. Grossman, C. Curiel-Lewandrowski, E. Y. Chu, M. E. Ming, K. Zhu, M. Brahmbhatt, V. Balakrishnan, M. J. Davis, Z. Wolner, N. Fleming, L. K. Ferris, J. Nguyen, O. Trofymenko, Y. Liu and S. C. Chen (2018) Risk of subsequent cutaneous melanoma in moderately dysplastic nevi excisionally biopsied but with positive histologic margins. *JAMA Dermatol.* **154**, 1401–1408.
39. Argenziano, G., S. Puig, Z. Iris, F. Sera, R. Corona, M. Alsina, F. Barbato, C. Carrera, G. Ferrara, A. Guilabert and D. Massi (2006) Dermoscopy improves accuracy of primary care physicians to triage lesions suggestive of skin cancer. *J. Clin. Oncol.* **24**, 1877–1882.